ACCSCIENCE PUBLISHING

International Journal of AI for Materials and Design

ORIGINAL RESEARCH ARTICLE

Structural health monitoring of metal structures using an improved carbon nanotube bucky paper sensor and LSTM neural network

Faeez Masurkar*

Department of Engineering, Faculty of Engineering and IT, The British University in Dubai, Dubai International Academic City, Dubai, United Arab Emirates

Abstract

In this paper, an improved fabrication method is presented for fabricating carbon nanotube (CNT) based multi-functional bucky paper (CNT-BP) sensors that will be primarily used for adaptive sensing in structural health monitoring applications. A large number of BPs were fabricated using multi-walled CNTs with varying methanol-CNT compositions, sonication times, temperatures, curing durations, membrane thicknesses, and electrode placements to determine the optimal configuration for large-scale production. The obtained optimal configuration of the ingredients that yields an adequate sensitivity and ductility of the CNT-BP was then employed for measuring the crack propagation behavior in the fatigued samples. Further, a long short-term memory (LSTM)-based neural network was proposed for prognosis in a metallic plate with fatigue crack propagation. The actual crack lengths of the fatigue crack obtained by the high-speed digital camera were correlated with that predicted by the CNT-BP-based model and LSTM, showing good agreement. Thus, the present study demonstrates that the proposed improved method of CNT-BP is highly efficient in the diagnosis and prognosis of fatigue cracks in metallic structures.

Keywords: Carbon nanotube; Bucky paper; Adaptive sensing; Piezo-resistivity; Fabrication; Structural health monitoring; Metallic structures

***Corresponding author:**
Faeez Masurkar
(faeez.masurkar@buid.ac.ae)

Citation: Masurkar F. Structural health monitoring of metal structures using an improved carbon nanotube bucky paper sensor and LSTM neural network. *Int J AI Mater Design*. 2025;2(3):78-87. doi: 10.36922/IJAMD025310028

Received: July 29, 2025

Revised: September 2, 2025

Accepted: September 8, 2025

Published online: September 23, 2025

1. Introduction

Metallic structures undergo a variety of degradation mechanisms, such as fatigue cracks, notches, and corrosion. These cracks under the action of loads can propagate further and result in the breakage of the structure. Therefore, it is extremely important to investigate the health status of these structures from time to time to ensure their structural integrity is above the required limit and avoid potential mishaps.[1-3] These can be achieved in several ways by employing different types of sensors. One of the sensors that facilitate self-sensing of the material changes is the use of a carbon nanotube (CNT)-based bucky paper (BP) sensor for measuring the crack propagation in specimen. This type of sensor also can be used in numerous other applications as found in literature.

Luo *et al.*[4] developed an *in situ* structural health monitoring system for polymer matrix composites using BP embedded between the laminas. The BP-based testing is widely used for damage and load sensing in aerospace and defense applications due to

its low density, high electrical conductivity, and significant load sensitivity. Wang *et al.*[5] correlated the electrical resistance of BP sensor with the strain for monitoring the health of composite structures. It can be seen that the BP sensor has very high strain sensitivity in the static tensile test. Lu *et al.*[6] employed an omnidirectional, nanomaterial-based sensor for impact damage detection in composite structures. The influence of both tensile and low-velocity impact on the BP sensors was also further investigated. Lu *et al.*[7] proposed a real-time monitoring of resin infiltration process in vacuum-assisted molding of composites with CNT-BP sensors. Her *et al.*[8] employed CNT-BP sensor on a complex surface for monitoring the strain and temperature at the critical areas of the sample. Yee *et al.*[9] developed an improved fabrication process for enhancing the sensitivity of the BP sensor for strain monitoring applications. Yang *et al.*[10] proposed a flexible, lightweight, and low-thickness BP sensor for high-performance electromagnetic interference shielding materials for catering to the demand for smart and wearable electronic devices. De Paula Santos *et al.*[11] investigated the effect of incorporating CNT-BP on the interlaminar fracture toughness by testing under cyclic loading in Mode I and II. Ahmed *et al.*[12] investigated the efficiency of a CNT sensor to detect and monitor fatigue crack initiation and propagation in metal structures. The sensor consisted of a non-woven carrier fabric with a thin film of CNT that is superglued to the structure's surface using an epoxy adhesive. Jiang *et al.*[13] employed CNT-BP sensors to monitor the structural health status of composite structures subjected to ambient vibration condition. Hehr *et al.*[14] employed CNT thread in unidirectional glass fiber composites to identify the onset of track crack growth, matrix cracking, and differentiate between crack breathing and closing states. This information is obtained by analyzing the resistance response of the thread with a simple Wheatstone bridge circuit and a low-speed data acquisition system. Ribeiro *et al.*[15] reviewed the general characteristics, physical properties, and processing conditions of CNT-BP and its polymer composites. Wan *et al.*[16] investigate the *in situ* monitoring of Mode I interlaminar crack propagation behavior in woven glass fiber-reinforced epoxy (WGF/epoxy) composite laminates. Lecompte *et al.*[17] employed two different optical measurement techniques for the detection of cracks at the surface of a concrete beam being subjected to flexural loading. The primary aim of the study was to examine which of the two methods appears to be the most suitable for crack detection. Moreover, it was shown that it is possible to detect the appearance and evolution of cracks, even before the cracks become visually detectable. Ashrafi *et al.*[18] focused on the application of epoxy nanocomposite thin film sensors for continuous monitoring of crack evolution in metallic structures. The primary aim was to monitor the resistance change in these nanocomposite films, as cracks develop and propagate in the metallic host structure. Bian *et al.*[19] proposed a facile technique to enhance performance of carbon fiber composites through interlaminar insertion of aligned CNT sheets. The inserted CNT sheets also provide electrical conductivity in the composites even at a low CNT loading below the electrical percolation threshold established for CNT-filled composites. Lin *et al.*[20] presented a flexible CNT-based strain sensor that has a significant potential for applications in human motion monitoring systems and electronic skins in water. Olson *et al.*[21] investigated a CNT-based sensor to detect crack propagation in aluminum structures underneath composite patching. Initial tests were conducted to determine the correct procedure and materials to properly fabricate a highly sensitive CNT-based sensor.

The present work proposes an improved fabrication process for the CNT-BP for measuring the fatigue crack propagation in a metallic specimen under uniaxial loading. First, an optimal composition for different ingredients required for fabricating CNT-BP was obtained and further optimized for its sensing architectures. This includes the CNT-BP sensor size, sensing locations, and number of sensing points, and the silver ink electrode placement. It is found that the fabricated CNT-BP sensor has enhanced sensitivity and has adequate ductility so that it can be easily superglued to the test structure. Moreover, a strong correlation was observed among the actual crack lengths measured by a high-speed optical camera, the crack estimates based on CNT-BP resistance, and the predictions from the long short-term memory (LSTM) neural network. This shows that CNT-BP has promising potential for fatigue crack prognosis and diagnosis without the need for complex equipment, signal processing, and measurement units.

The rest of the paper is organized as follows. The theoretical model for prediction of crack length is presented in Section 2, while the CNT-BP fabrication process is detailed in Section 3. Section 4 discusses the LSTM neural network for prognosis of a metallic plate with fatigue crack propagation, and the experimental study is discussed in Section 5. The results obtained are discussed in Section 6, and lastly, the concluding remarks and future study are given in Section 7. The following section discusses the theoretical model for crack length prediction based on the measurement of resistance change of CNT-BP as a function of fatigue cycles.

2. Theoretical model for prediction of crack length

A measurement model to correlate between the fatigue crack at any instant of time and the electrical resistance

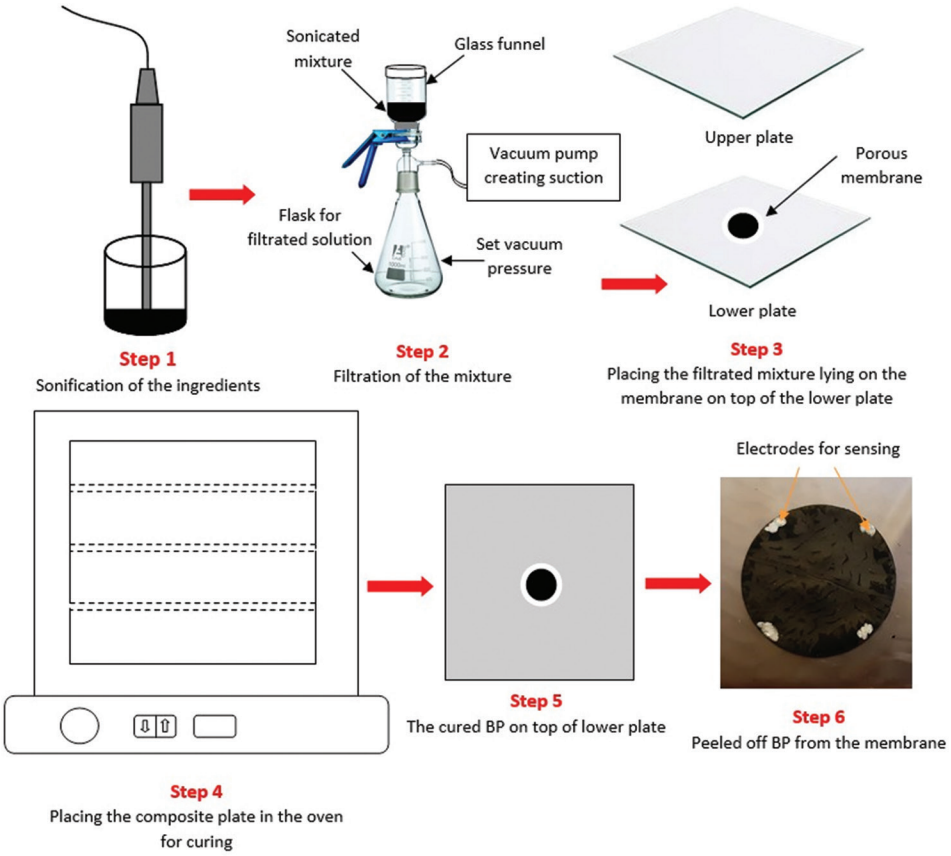

Figure 1. Schematic of the complete setup employed for fabrication of CNT-BP.
Abbreviations: BP: Bucky paper; CNT: Carbon nanotube.

of the CNT-BP specimen is required. This model must consider the dimensions of the CNT-BP specimen, positioning of the silver ink electrode, baseline resistance, and subsequent changes in the resistivity due to fatigue loading. Since the loading is purely uniaxial and with Mode I, the crack growth is perpendicular to the direction of the uniaxial loading. The relation between the resistance of the BP and crack length can be established as follows,

$$R = \frac{\rho d}{t(D - \hat{a})} \quad \text{(I)}$$

which can be re-written as:

$$\hat{a} = D - \left(\frac{\rho d}{Rt}\right) \quad \text{(II)}$$

In the above equations, R is the measured electrical resistance of the CNT-BP, ρ is the resistivity of embedded CNT-BP, d is the length of CNT-BP between electrodes, t is the thickness of CNT-BP, D is the diameter of omnidirectional CNT-BP specimen, and $\hat{a}$ is the estimated fatigue crack length.

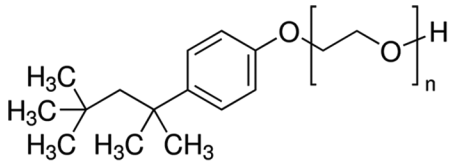

Figure 2. Chemical structure of Triton X-100

3. Fabrication process of the CNT-BP membrane

The improved fabrication process used to prepare the BP membranes is shown schematically in Figure 1. The key ingredients used were multi-walled CNTs (MWCNTs), Triton X-100 (t-octylphenoxypolyethoxyethanol, polyethylene glycol tert-octylphenyl ether), methanol, nitric acid solution, and distilled water. Triton X-100 was procured through Sigma-Aldrich (USA), and its chemical structure is shown Figure 2. The MWCNT used were obtained from US Research Nanomaterials (Houston, Texas, USA). These CNTs have an average outer diameter of 10–30 nm with an average length of 15–30 μm and purity of 90% as per the specifications given by supplier.

The properties of CNTs are as follows: density of 2100 kg/cu.m, specific surface area of $200\ m^2/g$, and conductivity $>10^4 S/m$. The experimental setup for fabricating the CNT-BP consists of a sonicator, a filtering setup equipped with vacuum pump that creates the controlled and pre-determined vacuum for sucking the liquid, metallic plates that house the CNT-BP, a vacuum oven that is used to cure the CNT-BP, and the CNTs. The filter membrane is Deschem with an outer diameter (OD) of 150 mm and a membrane of cellulose acetate with thickness of 45 μm.

For the fabrication procedure, 300 mg of MWCNT were mixed in 30 mL of methanol solution and 3 mL of Triton X-100, followed by 30 mL of distilled water. This high-concentration mixture was thoroughly ultrasonicated with a tip sonicator. The sonification time was set to roughly 30 mins. The process also assists in evaporation of methanol solvent and yields a highly viscous slurry for further process. Before transferring the slurry to the filtration process, a glass rod was used to stir the mixture to improve the overall homogeneity. Once the CNT-BP membrane is cured in the oven, it is peeled off from the membrane and is ready to use for testing purposes.

The major contribution of this paper is the development of improved fabrication process of CNT-BP, which was achieved by obtaining an optimal configuration of ingredients by conducting a significant number of trials. The use of Triton X-100 facilitates the production of a highly ductile and sensitive CNT-BP. The excess amount of Triton X-100 after curing was then washed off with nitric acid. Validated in our laboratory for multiple times, this procedure yields a CNT-BP that has significant potential for structural health monitoring applications of isotropic or anisotropic materials.

4. LSTM neural network

The LSTM neural network was employed in this study for prognosis of the metallic plate under fatigue loading. This type of neural network accurately predicts the time-series data with information fusion capabilities exhibiting multiple-input multiple-output (MIMO) and left/right cracks under propagation. It also facilitates the alleviation of the gradient vanishing problem in recurrent neural network by incorporating LSTM unit, thereby having enhanced prediction accuracy.[22-25] A schematic illustration of the LSTM model is shown in Figure 3. Crack propagation under increasing fatigue cycles is a complicated process; therefore, surrogate models based on machine learning are gaining attention for predicting crack length. It also facilitates automatic damage-sensitive feature extraction through the data pattern analysis in the measured experimental data.

Figure 3 shows the repeating module of an LSTM and how the information flows across the sequential time steps. In the figure, x_t is the input at time t, y_{t-1} is the hidden state from the previous step, y_t is the hidden state at the current time step (output of the LSTM). There are four interacting layers in LSTM controlling the information flow. The forget gate, whose operation is given as:

$$f_t = \rho(W_f \cdot [y_{t-1}, x_t] + b_f) \quad \text{(III)}$$

where W_f and b_f are the weight and bias parameters, respectively, and ρ is the sigmoid activation function. The function decides what portion of the previous cell state should be forgotten. The input gate is given as,

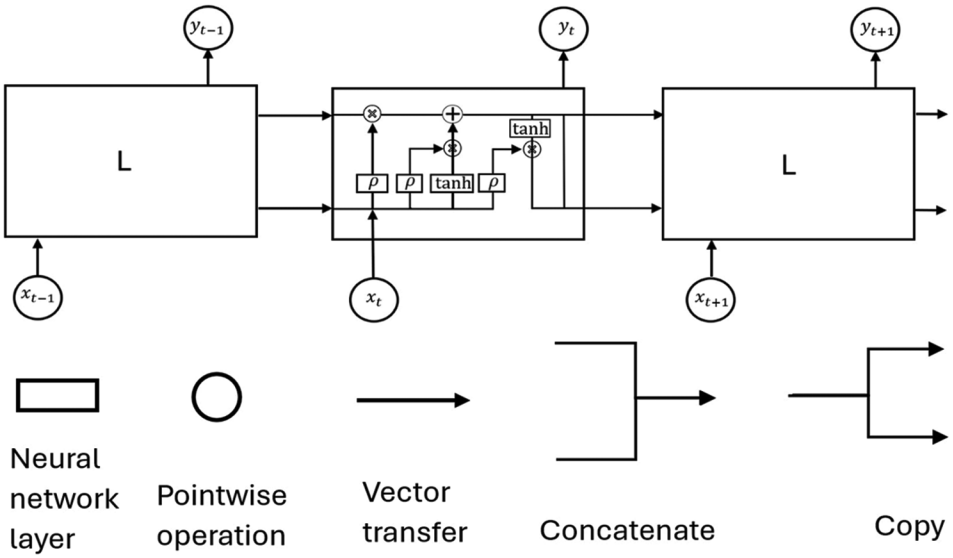

Figure 3. Schematic illustration of the long short-term memory (LSTM) model encompassing the repeating module and four interacting layers.[26]

$$i_t = \rho(W_i \cdot [y_{t-1}, x_t] + b_i) \quad \text{(IV)}$$

The input gate decides how much of the new information should be added to the cell state. The candidate cell state can be given as:

$$C_t = \tanh(W_c \cdot [y_{t-1}, x_t] + b_c) \quad \text{(V)}$$

The cell state decides what part of the new candidate values potentially be added to the cell state. The output gate is given as:

$$o_t = \rho(W_0 \cdot [y_{t-1}, x_t] + b_0) \quad \text{(VI)}$$

The output gate decides what part of the cell state will be the output at the hidden state h_t. The cell state is updated in two steps:

$$C_t = f_t \cdot C_{t-1} + i_t \cdot \widehat{C_t} \quad \text{(VII)}$$

The forget gate controls what to keep or discard from the past, and the input gate and candidate state add new information. Finally, the hidden state or the output of the LSTM cell is computed as:

$$h_t = o_t \cdot \tanh(C_t) \quad \text{(IX)}$$

This ensures that the hidden state is regulated and is not just the raw memory value. The experimental study is discussed in the following section.

5. Experimental study

In this section, the details of the experimental study related to the metallic plate testing with CNT-BP are given. The details of the testing scheme and experimental setup are given in the following subsection.

5.1. Experimental setup for testing

The loading mechanism applied to the test samples is shown in Table 1. Three types of fatigue tests were conducted, and test 1 shows the total life of the sample which resulted in its breakage. The samples were fatigued with the help of an accelerated fatigue machine (MTS 370) with a load capacity 25 kN. The specimens were fatigued under tension-tension stress-controlled condition with stress ratio of 0.1. Further, the complete components used in the experimental study are shown in Figure 4. A customized attachment holding the specimen within the upper and lower jaws of the MTS 370 was fabricated. A small hole was created with two notches on its periphery in horizontal direction to increase stress concentration and facilitate crack initiation and stable propagation with an increase of fatigue cycles.[27-29]

Two CNT-BPs of same shape and size were superglued near these notch locations, as shown in Figure 4. The outer periphery of CNT-BP was well aligned with the location of the notch, where crack is about to initiate. Moreover, an optical camera was employed to measure the actual crack length from the backside of the sample as a function of fatigue cycles. The purpose of fatigue test 1 is to determine the life of specimen. Tests 2 and 3 were employed for measuring resistance change of CNT-BP as a function of fatigue cycles. For brevity, only the results from test 3 are shown herein. Nevertheless, the nature of the results of CNT-BP resistance change measurement and crack length prediction is almost similar. The results and discussions of the study are presented in the following section.

Table 1. The loading mechanism for the fatigue test

Loading conditions	Fatigue test 1	Fatigue test 2	Fatigue test 3
Load	1–10 kN; R=0.1	1.5–15 kN; R=0.1	1.5–15 kN; R=0.1
Loading frequency	10 Hz	10 Hz	10 Hz
Fatigue life	Test aborted at 760,000 cycles resulting in breakage	115,087 cycles	119,652 cycles

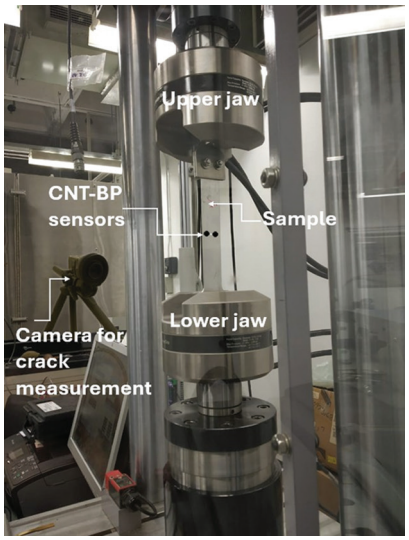

Figure 4. Experimental arrangement for fatigue crack propagation measurement using an optical camera and CNT-BP sensors
Abbreviations: BP: Bucky paper; CNT: Carbon nanotube

6. Results and discussion

The dimensions and intrinsic resistance of each BP were measured using a multimeter before being affixed to the specimen with superglue. These resistance values of the BP serve as the baseline measurements, providing a reference for all future measurements. The dimensions between each of the silver ink electrodes were also measured, forming a part of the theoretical model and accounted by parameter d in Equations I and II. It is worth noting that before affixing the CNT-BP to test specimen, the intrinsic values of the BP

serving as the baseline measurements were measured at five different times and with different multimeters. However, a single stable value was noted in each case, confirming that the baseline measurements are reproducible. Several fatigue tests were conducted on different Al 7075 specimens as detailed in Table 1. The stable resistance of the CNT-BP affixed on the left of the hole is 5.6 Ω, whereas that on the right is 5.8 Ω, as shown in Figure 5A and B. Only the baseline value measured from CNT-BP placed near the right hole is shown for demonstration purposes. The specimens were loaded to different fatigue cycles, and the resistance values of the BP were obtained simultaneously. However, the values were recorded at regular intervals. These resistance values were further used in Equations I and II to determine the correlated fatigue crack length, which is shown in Figures 6A and B for the left and right cracks, respectively.

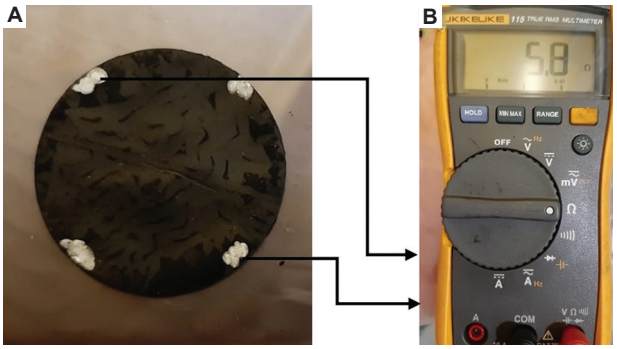

Figure 5. The improved bucky paper (A) and its measured resistance (B)

It can be seen that the error on the right crack measurement is less than that on the left crack. It could be because the initial resistance of right BP is slightly higher than that of the left BP, demonstrating a slightly higher sensitivity. Furthermore, the trend of the crack size for different fatigue cycles is captured accurately. Nevertheless, the variation of resistance for different fatigue cycles is also shown in Figure 7A and B, and the trend of this variation is in line with those obtained in related literature. Finally, the

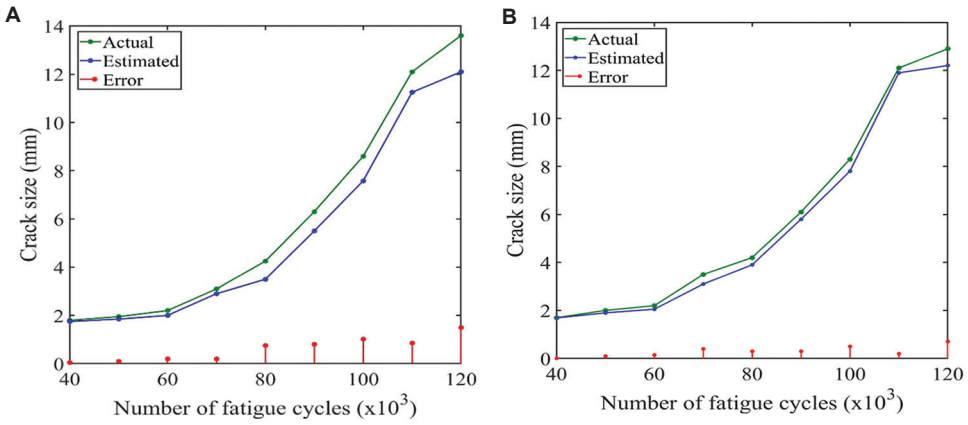

Figure 6. The propagation of crack size versus thousands of cycles: (A) Left crack, and (B) right crack.

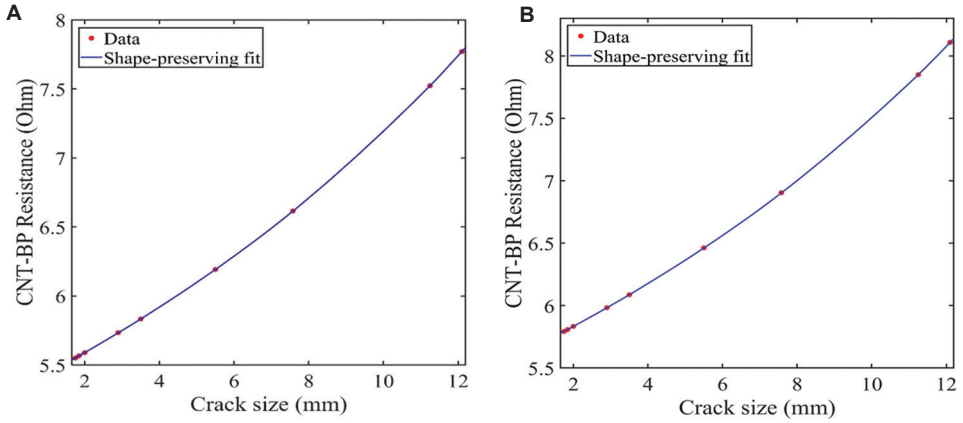

Figure 7. Variation of CNT-BP resistance with the propagation of crack: (A) Left crack, and (B) right crack
Abbreviations: BP: Bucky paper; CNT: Carbon nanotube.

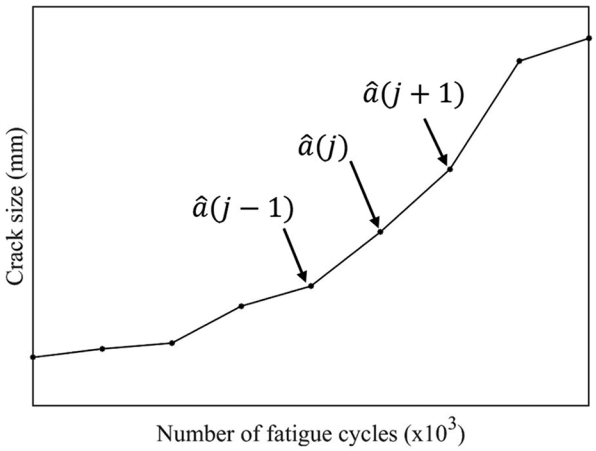

Figure 8. Crack size propagation as a function of fatigue cycles

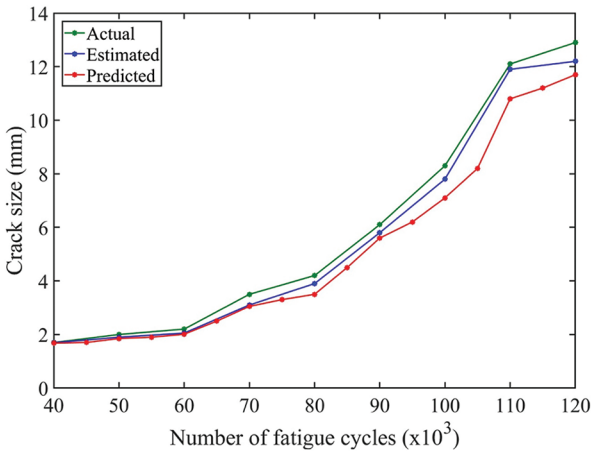

Figure 9. The variation of actual, estimated and predicted crack size versus the fatigue cycles

trend appears to increase approximately linearly with the number of cycles, suggesting a linear correlation between crack size and fatigue cycles. It can also be seen that for lower fatigue cycles, the crack size is not that noticeable and so is the change of resistance of CNT-BP demonstrating an approximate flat line with marginal error. This is seen for both the CNT-BPs placed on the left and right side of the hole.

The prognosis of the metallic plate with an increasing fatigue crack was obtained with the LSTM neural network. An illustrative relationship between crack size and increasing fatigue cycles is shown in Figure 8. Further, it is evident that the time transient crack size propagation is dependent on the previous crack size, fatigue cycle, and the rate at which the crack propagates with respect to fatigue cycle is shown in Table 2, and mathematically, this can be represented by Equation X:[30-32]

$$\hat{a}(j+1) = f\left(\ldots, \hat{a}(j), N(j), \frac{d\hat{a}}{dN(j)}\right) \quad \text{(X)}$$

The estimated values of the crack size based on the change in resistance measurement were used for training the LSTM model. The actual values obtained from the optical camera were only used as a reference for those obtained from measuring the change of resistances in CNT-BP as a function of fatigue cycles. Therefore, they were not used for training the LSTM model. The trained LSTM model was then used to predict the crack size as a function of fatigue cycles. The results, shown in Figure 9, demonstrate not only high prediction accuracy but also a strong alignment with the overall trend of crack growth over fatigue cycles. The concluding remarks and future studies are discussed in the following section.

Table 2. Time series data for crack propagation as a function of fatigue cycles

Time step	…	$j-1$	J	$j+1$	…
$\hat{a}$	⋯		$\hat{a}(j)$	$\hat{a}(j+1)$	⋯
N	…	$N(j-1)$	$N(j)$	$N(j+1)$	…
$\frac{d\hat{a}}{dN}$	⋯	$\frac{d\hat{a}}{dN(j-1)}$	$\frac{d\hat{a}}{dN(j)}$	$\frac{d\hat{a}}{dN(j+1)}$	⋯

7. Concluding remarks and future study

The present study focuses on the development of an improved method for the fabrication of CNT-BP membranes that can be used as self-sensing material with an application for structural health monitoring of metallic plate structures which are subjected to fatigue loading. A significant number of trials were conducted to determine the optimal configuration of the ingredients to fabricate the CNT-BP that has adequate ductility and enhanced sensitivity. The optimized CNT-BPs were superglued to the fatigued test specimens to measure the change in resistance values of the CNT-BP as a function of fatigue cycles. The measured resistance values were then used to calculate the fatigue crack sizes. Moreover, a high-speed optical camera was employed to measure the actual size of the fatigue crack. A good correlation was observed between the actual size of the crack measured by the optical camera and the one calculated using the established theoretical model based on the change in resistance of the CNT-BP and that predicted from the LSTM model. Thus, the obtained results demonstrated the promising potential of CNT-BP for health monitoring applications. The major findings and outcomes from the present study are outlined below:

(i) The ductility of the fabricated CNT-BP is enhanced with the improved fabrication process. This is paramount because if the CNT-BP is brittle, it can be difficult to handle and may break while being glued to the test specimen. Furthermore, it may be relatively easy to superglue the ductile CNT-BP to the test specimen by tapping to ensure a uniform attachment of CNT-BP to the specimen, avoiding any voids formation at the interface.
(ii) The sensitivity of the fabricated BP is enhanced with the improved fabrication process, as demonstrated by the marginal error between the actual and predicted results of fatigue crack. The piezoresistivity is improved up to 5.8 Ω compared to the earlier reported values between 4 Ω and 5 Ω.
(iii) The error analysis shows the potential of CNT-BP in crack length estimation with enhanced accuracy and sensitivity.
(iv) For higher crack length estimation, an approximate linear relationship seems to exist, indicating that the LSTM model can predict the trend with higher accuracy.
(v) The use of CNT-BP as a self-sensing material eliminates the need for sophisticated equipment and sensors, complex signal processing, and high computational resources. Further, CNT-BP can be easily affixed to the test structure, and changes in its electrical resistance can be readily measured.
(vi) The omnidirectional shape of the CNT-BP can facilitate the detection of cracks in different directions with higher sensitivity.

In contrast, the current work identified several limitations that could be explored in future studies. The limitations are as follows:

(i) Limited BP size due to the filter membrane size.

To yield CNT-BP with larger sizes, a flask with a bigger funnel width, membrane, and pore sizes must be employed during the fabrication process. This could also facilitate mass fabrication since smaller pieces with equal sizes and shapes can be cut out of the large BP, thereby reducing the fabrication time. The fabrication of BP into different shapes and sizes for future testing may lead to further overall optimization of the sensing architecture.

(ii) Different crack directions.

In this work, only the crack propagating perpendicular to the loading direction was considered. The CNT-BP must be tested for different crack directions to further investigate and confirm the reliability of its sensing efficiency and use in prognosis and diagnosis of fatigued specimens.

(iii) Different electrode arrangements for damage detection and quantification.

The electrode arrangements must be varied according to the location and direction of the crack propagation. This would give further insights for optimizing the sensing architecture for a specific application.

(iv) Obtaining readings at different load levels and directions.

In the present study, the load was tension-tension controlled at a specific loading frequency. In future work, both the loading amplitude and direction—ranging from tension to compression—and the loading frequency can be varied to further evaluate the reliability of CNT-BP in the prognosis and diagnosis of fatigue in specimens.

Acknowledgments

None.

Funding

None.

Conflict of interest

Faeez Masurkar is the Youth Editorial Board Member of this journal, but was not in any way involved in the editorial and peer-review process conducted for this paper, directly or indirectly.

Author contributions

This is a single-authored article.

Ethics approval and consent to participate

Not applicable.

Consent for publication

Not applicable.

Availability of data

The data presented in this study are available from the corresponding author on request.

References

1. Masurkar F, Tse PW, Yelve NP. Theoretical and experimental measurement of intrinsic and fatigue induced material nonlinearities using Lamb wave based nonlinearity parameters. *Measurement*. 2020;151:107148.

   doi: 10.1016/j.measurement.2019.107148

2. Tse P, Masurkar F, Yelve NP. Estimation of remaining useful life of fatigued plate specimens using Lamb wave-based nonlinearity parameters. *Struct Control Health Monit.* 2020;27(4):e2486.

   doi: 10.1002/stc.2486

3. Yelve NP, Masurkar F, Tse PW. Application of rayleigh wave-based nonlinearity parameter to estimate the remnant useful life of fatigued thick aluminum plates. *ISSS J Micro Smart Syst.* 2021;10(2):161-178.

doi: 10.1007/s41683-021-00074-5

4. Luo W, Liu Y, Saha M. CNT Bucky Paper Enhanced Sandwich Composites for In-Situ Load Sensing. In: *Proceedings of the ASME International Mechanical Engineering Congress and Exposition*. Vol. 58493. 2017. p. V014T11A044.

doi: 10.1115/IMECE2017-71550

5. Wang X, An B, Lu S, Ma K, Zhang L, Xu T. Electrical response of carbon nanotube buckypaper sensor subjected to monotonic tension, cycle tension and temperature. *Micro Nano Lett.* 2018;13(6):862-867.

doi: 10.1049/mnl.2017.0914

6. Lu S, Du K, Wang X, *et al*. Real-time monitoring of low-velocity impact damage for composite structures with the omnidirection carbon nanotubes' buckypaper sensors. *Struct Health Monit.* 2019;18(2):454-465.

doi: 10.1177/1475921718757937

7. Lu S, Yang X, Zhang L, *et al*. Real-time monitoring of resin infiltration process in vacuum assisted molding (VARI) of composites with carbon nanotube buckypaper sensor. *Mater Res Express.* 2019;6(11):115628.

doi: 10.1088/2053-1591/ab507b

8. Her SC, Hsu WC. Strain and temperature sensitivities along with mechanical properties of CNT buckypaper sensors. *Sensors (Basel)*. 2020;20(11):3067.

doi: 10.3390/s20113067

9. Yee MJ, Mubarak NM, Khalid M, Abdullah EC, Jagadish P. Synthesis of polyvinyl alcohol (PVA) infiltrated MWCNTs buckypaper for strain sensing application. *Sci Rep.* 2018;8(1):17295.

doi: 10.1038/s41598-018-35638-3

10. Yang R, Gui X, Yao L, *et al*. Ultrathin, lightweight, and flexible CNT buckypaper enhanced using MXenes for electromagnetic interference shielding. *Nanomicro Lett.* 2021;13:66.

doi: 10.1007/s40820-021-00597-4

11. De Paula Santos LF, Monticeli FM, Ribeiro B, Costa ML, Alderliesten R, Botelho EC. Effect of carbon nanotube buckypapers on interlaminar fracture toughness of thermoplastic composites subjected to fatigue tests. *Int J Fatigue*. 2025;195:108868.

doi: 10.1016/j.ijfatigue.2025.108868

12. Ahmed S, Schumacher T, Thostenson ET, McConnell J. Performance evaluation of a carbon nanotube sensor for fatigue crack monitoring of metal structures. *Sensors (Basel)*. 2020;20(16):4383.

doi: 10.3390/s20164383

13. Jiang XW, Wang Z, Lu SW, *et al*. Vibration monitoring for composite structures using buckypaper sensors arrayed by flexible printed circuit. *Int J Smart Nano Mater.* 2021;12(2):198-217.

doi: 10.1080/19475411.2021.1910874

14. Hehr A, Schulz M, Shanov V, Song Y. Micro-crack detection and assessment with embedded carbon nanotube thread in composite materials. *Struct Health Monit.* 2014;13(5):512-524.

doi: 10.1177/1475921714532987

15. Ribeiro B, Botelho EC, Costa ML, Bandeira CF. Carbon nanotube buckypaper reinforced polymer composites: A review. *Polímeros*. 2017;27(3):247-255.

doi: 10.1590/0104-1428.03916

16. Wan Y, Yang H, Tian Z, *et al*. Mode I interlaminar crack length prediction by the resistance signal of the integrated MWCNT sensor in WGF/epoxy composites during DCB test. *J Mater Res Technol.* 2020;9(3):5922-5933.

doi: 10.1016/j.jmrt.2020.03.119

17. Lecompte D, Vantomme J, Sol H. Crack detection in a concrete beam using two different camera techniques. *Struct Health Monit.* 2006;5(1):59-68.

doi: 10.1177/1475921706057982

18. Ashrafi B, Johnson L, Martinez-Rubi Y, Martinez M, Mrad N. Single-walled carbon nanotube-modified epoxy thin films for continuous crack monitoring of metallic structures. *Struct Health Monit.* 2012;11(5):589-601.

doi: 10.1177/1475921712449509

19. Bian N, Ren Y, Shrivastava A, *et al*. Enhancing the interlaminar adhesion of carbon fiber composites via carbon nanotube sheets. *Acad Mater Sci*. 2024;1(2).:1-11.

doi: 10.20935/AcadMatSci6206

20. Lin H, Zhang C, Liao N, Zhang M. Microcracked strain sensor based on carbon nanotubes/copper composite film with high performance and waterproof property for underwater motion detection. *Compos Part B Eng.* 2023;254:110574.

doi: 10.1016/j.compositesb.2023.110574

21. Olson TM, Kwon YW, Hart DC, Loup DC, Rasmussen EA. Carbon nanotube based sensor to monitor crack growth in cracked aluminum structures underneath composite patching. *Appl Compos Mater.* 2015;22(5):457-473.

doi: 10.1007/s10443-014-9417-0

22. Abbasi A, Nazari F, Nataraj C. Application of long short-term memory neural network to crack propagation prognostics. In: *Proceedings of the 2020 IEEE International Conference on Prognostics and Health Management*

(ICPHM); 2020. p. 1-6.

doi: 10.1109/ICPHM49022.2020.9187033

23. Pan Y, Khodaei ZS, Aliabadi FM. In-service fatigue crack monitoring through baseline-free automated detection and physics-informed neural network quantification. *NDT E Int.* 2025;153:103360.

doi: 10.1016/j.ndteint.2025.103360

24. Shin H, Yoon T, Yoon S. Fatigue life predictor: Predicting fatigue life of metallic material using LSTM with a contextual attention model. *RSC Adv.* 2025;15(20):15781-15795.

doi: 10.1039/d5ra01578b

25. Giannella V, Bardozzo F, Postiglione A, Tagliaferri R, Sepe R, Armentani E. Neural networks for fatigue crack propagation predictions in real-time under uncertainty. *Comput Struct.* 2023;288:107157.

doi: 10.1016/j.compstruc.2023.107157

26. Colah. *Understanding LSTMs*; 2015. Available from: https://colah.github.io/posts/2015-08-Understanding-LSTMs/ [Last accessed on 2025 Sep 19].

27. Masurkar F, Tse P. Theoretical and experimental evaluation of the health status of a 1018 steel I-beam using nonlinear rayleigh waves: Application to evaluating localized plastic damage due to impact loading. *Ultrasonics*. 2020;108:106036.

doi: 10.1016/j.ultras.2019.106036

28. Yelve NP, Tse PW, Masurkar F. Theoretical and experimental evaluation of material nonlinearity in metal plates using Lamb waves. *Struct Control Health Monit.* 2018;25(6):e2164.

doi: 10.1002/stc.2164

29. Masurkar F, Tse P, Yelve NP. Evaluation of inherent and dislocation induced material nonlinearity in metallic plates using Lamb waves. *Appl Acoust.* 2018;136:76-85.

doi: 10.1016/j.apacoust.2018.02.011

30. Xu N, Fu Z, Wang Y, Shen X. Study on the short fatigue crack initiation and propagation behavior of 42CrMo. *Adv Mech Eng.* 2022;14(9):1-9.

doi: 10.1177/16878132221119928

31. Ibrahim MFE, Miller KJ. Determination of fatigue crack initiation life. *Fatigue Fract Eng Mater Struct.* 1979;2(4):351-360.

doi: 10.1111/j.1460-2695.1979.tb01093.x

32. Wang H, Liu X, Wang X, Wang Y. Numerical method for estimating fatigue crack initiation size using elastic-plastic fracture mechanics method. *Appl Math Model.* 2019;73:365-377.

doi: 10.1016/j.apm.2019.04.010